






Article

Exponential Curve-Based Control Strategy for Auxiliary Equipment Power Supply Systems in Railways

Shoeb Azam Farooqui ¹, Chang-Hua Lin ¹, Shiue-Der Lu ^{2,*}, Hwa-Dong Liu ³, Adil Sarwar ⁴
and Liang-Yin Huang ⁵

¹ Department of Electrical Engineering, National Taiwan University of Science and Technology, Taipei 106, Taiwan

² Department of Electrical Engineering, National Chin-Yi University of Technology, Taichung 411, Taiwan

³ Undergraduate Program of Vehicle and Energy Engineering, National Taiwan Normal University, Taipei 106, Taiwan

⁴ Department of Electrical Engineering, ZHCET, Aligarh Muslim University, Aligarh 202002, India

⁵ Graduate Institute of Manufacturing Technology, National Taipei University of Technology, Taipei 106, Taiwan

* Correspondence: sdl@ncut.edu.tw; Tel.: +886-4-23924505 (ext. 7260)

Abstract: An exponential curve-based (ECB) control strategy has been proposed in this paper. The proposed ECB control strategy is based on the growth and decay of charge in the series RC circuit and the harmonic elimination by detecting the Fourier expansion series of the auxiliary equipment power supply system's (AEPSS) three-phase output voltage level. It can quickly adjust each duty cycle to the best value for driving the isolated three-phase inverter (ITPI) and produce a three-phase 380 V_{AC}/60 Hz output. A comparison of the AEPSS output performance using the traditional voltage cancellation method (VCM) and the proposed ECB control strategy was performed. The hardware implementation of the system was performed on the prototype developed in the laboratory. These control strategies are tested under three conditions, i.e., (i) V_i = 550 V_{DC}. (ii) V_i = 750 V_{DC}. (iii) V_i = 800 V_{DC}. The total harmonic distortion (THD) is 13.7%, 14.5%, and 14.9%, and the output voltage V_o is 372.3 V_{AC}, 377.3 V_{AC}, and 385.3 V_{AC} using the traditional control strategy at three test conditions, respectively. However, the THD is 7.2%, 7.8%, and 8.0%, and the output voltage V_o is 382.2 V_{AC}, 381.2 V_{AC}, and 381.9 V_{AC} using the proposed ECB control strategy under the test conditions. It is obvious from the hardware results that the output voltage harmonics and output voltage level for the proposed ECB control strategy are superior to the traditional VCM. The voltage produced from the AEPSS using the proposed ECB control strategy is more stable and has better quality. In addition, the filter size is also reduced.

Keywords: auxiliary equipment power supply system; exponential curve-based control strategy; rail vehicles; isolated three-phase inverter



Citation: Farooqui, S.A.; Lin, C.-H.; Lu, S.-D.; Liu, H.-D.; Sarwar, A.; Huang, L.-Y. Exponential Curve-Based Control Strategy for Auxiliary Equipment Power Supply Systems in Railways. *Processes* **2023**, *11*, 1285. <https://doi.org/10.3390/pr11041285>

Academic Editor: Hsin-Jang Shieh

Received: 28 February 2023

Revised: 14 April 2023

Accepted: 17 April 2023

Published: 20 April 2023



Copyright: © 2023 by the authors. Licensee MDPI, Basel, Switzerland. This article is an open access article distributed under the terms and conditions of the Creative Commons Attribution (CC BY) license (<https://creativecommons.org/licenses/by/4.0/>).

1. Introduction

Fossil fuel-based vehicles have been used for transportation for centuries. Fossil fuels such as coal, diesel, and natural gas resources are limited, and their combustion emits CO₂, which leads to air pollution and the greenhouse effect [1–4]. It has severe impacts on human health as well as global climate change. Therefore, their rapid replacement by electric-powered automobiles is accelerating, and the demand for electric vehicles is increasing at a rapid pace [5]. EVs are dominating the market because of their low operating and maintenance cost, zero-tailpipe emission, and high efficiency. The electrification of railways is a step in the direction of achieving sustainable growth and development [6]. Rail transport is one of the most convenient and smoothest modes of land transportation. It provides convenient transportation for people, contributes to reducing environmental concerns, helps to improve traffic congestion, and saves the public time and money [7,8]. Railway electrification has not only reduced environmental concerns but also improved

railway performance and service quality. With the advancement of science and technology, several additional services and systems have been adopted in the railways to fulfill the basic requirements of passengers during the journey. Thus, making the journey more convenient and pleasant.

Electric rails are more reliable, quieter, and more powerful than fuel-based trains [9]. In recent decades, there has been a steady growth in railway electrification. At present, more than two-fifths of all railway lines across the world have been electrified. Three basic criteria are used to categorize the electrical systems in electrified railways: (i) Contact point: third rail, fourth rail, or overhead line through a catenary. (ii) Current: Direct Current (DC) or Alternating Current (AC). (iii) Voltage: Level and frequency. Different zones need separate infrastructures and systems. Numerous voltage schemes are used for electrified railways globally [10]. Some of the standard and non-standard voltage schemes used in electrified railways are mentioned in Figure 1. This shows that the electrified railways either deploy a DC source or an AC source to power the train. The DC sources may have different values depending upon the schemes, which may be 600 V, 750 V, 1500 V, or 3000 V. Similarly, the AC source may have different values as well as different frequencies. It may be 15 kV and 16.7 Hz, 25 kV and 50 Hz, or 25 kV and 60 Hz [11]. Different schemes are used in different places. The 750 V_{DC} supply scheme has been adopted in this work.

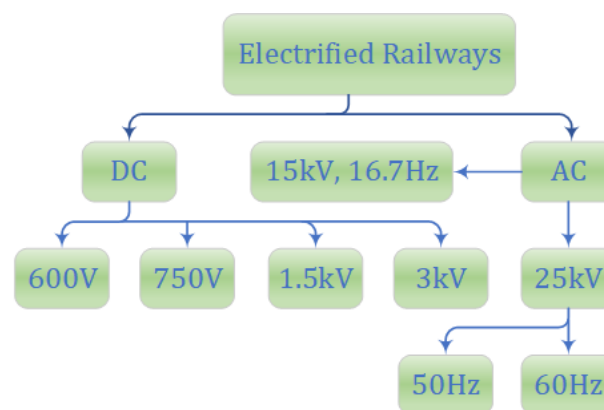


Figure 1. Several voltage schemes used in electrified railways.

An electrified railway has several electrical systems. The main electrical equipment of rail vehicles can be classified as auxiliary equipment power supply systems (AEPSS), propulsion systems (PS), lighting systems (LS), door systems (DS), and brake systems (BS) [12]. This study focuses on the rail vehicle AEPSS. An excellent AEPSS has great importance in rail vehicles. The AEPSS uses power electronic conversion technology to adopt a three-rail (TR) direct current (DC) source for producing a three-phase 380 V_{AC}/60 Hz output, a single-phase 110 V_{AC}/60 Hz, and a 110 V_{DC}. Since each item of equipment may have different input voltage specifications, therefore, the AEPSS produces numerous outputs to provide power to different appliances in the train. Several appliances, which are usually used to provide several facilities in the train for the convenience of the passengers, are air conditioning for cooling during the summer season, electric heaters for heating during cold periods, air compressors for the braking systems, and providing support to the suspension systems and other equipment, lighting inside the train coaches, and providing electrical supply to sockets for other utilities such as mobile phone and laptop charging, etc. First, a three-phase 380 V_{AC}/60 Hz power supply is needed for the rail vehicle's air conditioning, air compressor, and equipment blowers. Second, a single-phase 110 V_{AC}/60 Hz power is required for the cab electric heater and the vehicle socket. Thirdly, a 110 V_{DC} power source is required for the computer, headlight, lighting inside the cars of the train and the rail vehicle battery charging system. All of these required power supplies are produced by the rail vehicle AEPSS [13,14].

Figure 2 illustrates the architecture of the rail vehicle AEPSS. In this case, the load scale has been reduced to a lower value to perform experiment results in the laboratory. The 750 V_{DC} is supplied either from the third rail or from the overhead conductor depending upon the supply system. This is passed to the isolated three-phase inverter (ITPI) through the AEPSS input filter (L_i and C_i). The ITPI may either be the traditional or any other topology with some control strategy. However, the traditional ITPI has been used here because of its simplicity, fewer switch counts, and easy control. The Exponential curve-based (ECB) control strategy was proposed for controlling the output of the ITPI. The control strategy is based on the growth and decay of charge in the series RC circuit [15] and the harmonic elimination by detecting the Fourier expansion series of the AEPSS three-phase output voltage level [16,17]. The proposed ECB control strategy quickly adjusts each duty cycle to reach the best duty cycle and thus generates the best duty cycle for the ITPI driver. The output from ITPI is then passed through the output filter to obtain a high-quality and stable three-phase $380\text{ V}_{\text{AC}}/60\text{ Hz}$ output. Finally, the desired output from the AEPSS provides the power supply to the rail vehicle air conditioning, air compressor, equipment blower, electric heater, plug socket, and lighting inside the coaches of the train, etc. [18].

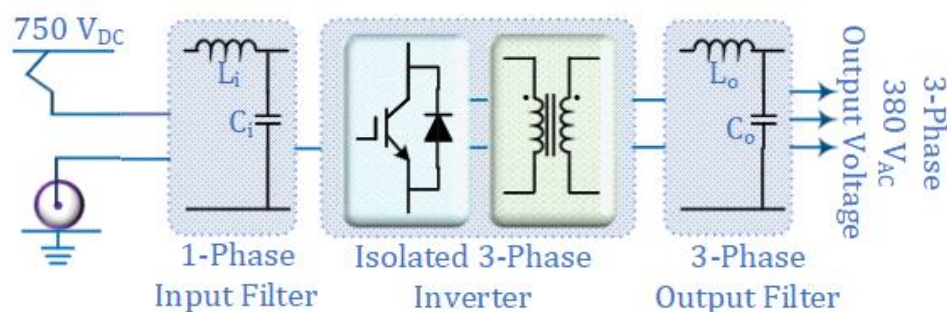


Figure 2. Architecture diagram of rail vehicle AEPSS.

The ECB control strategy has been proposed in this study. Its performance is then compared with the traditional voltage cancellation method (VCM) by providing the hardware results of both control strategies. The hardware result shows that the ECB control strategy performs better than the traditional VCM under the test conditions: 550 V_{DC} , 750 V_{DC} , and 800 V_{DC} . The THD is enormously reduced, and the output voltage V_o is more stable using the proposed ECB control strategy. Therefore, the system's performance is improved with reduced voltage harmonics using the proposed ECB control strategy.

2. AEPSS in Railways

Among the various electrical systems of rail vehicles, auxiliary equipment power supply systems (AEPSS) have been emphasized in this study. It is very important to have a good AEPSS in rail vehicles. An excellent AEPSS can provide a stable and high-quality voltage supply for the rail vehicle's electrical equipment, which will greatly improve the quality of passengers' rides and avoid the AEPSS problem of causing any inconvenience to passengers. The rail vehicles provide certain facilities for the convenience of passengers to make the journey more pleasant. Various appliances are installed inside the rail vehicle for this purpose. Specified power supplies are required to operate these appliances. Some appliances need AC power, while a few of them require DC power since the input power is 750 V_{DC} . Therefore, some kind of system must be provided that can be used to convert this power to the required specification. AEPSS are deployed in the rail vehicle to provide the power of the required specification for various appliances used inside the train. Some of the common appliances used inside the trains are air conditioners, air compressors, equipment blowers, batteries, and plug points for charging mobile phones, tablets, laptops, etc. Different appliances have different specifications. The AEPSS provides the specified power to operate those gadgets. Other trains may have different numbers of AEPSS

installed inside cars depending on the number of cars and the train size. Figure 3 shows the rail vehicle AEPSS configuration in a medium-capacity rail vehicle system. This medium-capacity rail vehicle system consists of four power cars. One set of the AEPSS is deployed for each power car that produces a three-phase $380\text{ V}_{AC}/60\text{ Hz}$ power source with a capacity of 60 kW [13], and the AEPSS output provides power to two air conditioning, an air compressor, and two equipment blowers traction container.

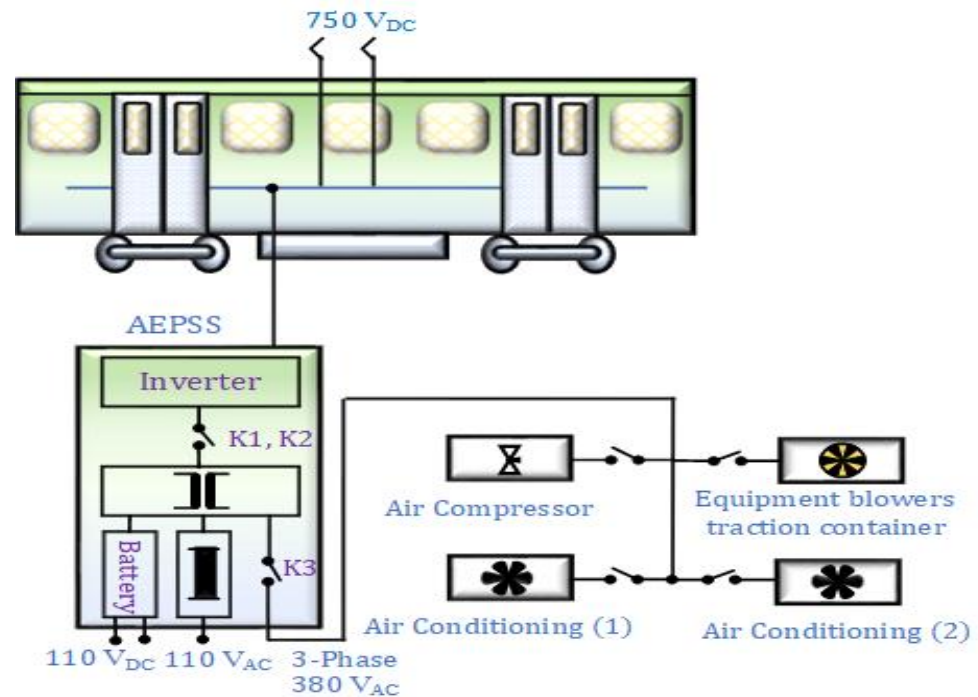


Figure 3. The rail vehicle AEPSS configuration in a medium-capacity rail vehicle system.

The heavy-capacity rail vehicle system consists of four power cars and two non-power cars, with a total of six cars. Electric multiple units (EMU) of a heavy-capacity rail vehicle system consist of two power cars and one non-power car. Two sets of the AEPSS are deployed for an EMU that provides a three-phase $380\text{ V}_{AC}/60\text{ Hz}$ power source with a capacity of 120 kW [14], and the AEPSS output provides power to six air conditioning, two air compressors, and four equipment blowers traction container.

A general AEPSS structure consists of an input filter, inverter, transformer, and output filter fed from an input DC supply to generate the desired output required for the load or other accessories. Figure 4 displays the schematic diagram of an AEPSS circuit structure in a single car. First, a 750 V_{DC} supply is provided to the AEPSS input. This 750 V_{DC} supply is provided through an overhead line conductor, which is received by AEPSS input using the catenary. This input supply is fed to the AEPSS input filter (L_i and C_i), which eliminates the noise from the 750 V_{DC} supply and stabilizes the voltage. Later, this input is converted to the three-phase alternating current power through an isolated three-phase inverter (ITPI). This ITPI may use any effective control strategy to produce three-phase AC power. A transformer is employed to provide the isolation. Furthermore, the three-phase alternating current power from ITPI output is filtered using the output filter (L_o and C_o). Finally, a high-quality and stable three-phase $380\text{ V}_{AC}/60\text{ Hz}$ is obtained from AEPSS output, fed to the air conditioning blowers induction motor (IM) and traction equipment blowers IM. The electrical specification of a general AEPSS is displayed in Table 1. It is evident from the table that the input voltage ranges from 550 V_{DC} to 800 V_{DC} while the output voltage is 3 phase 380 V_{AC} with a frequency of 60 Hz . Additionally, the system power is 30 kW .

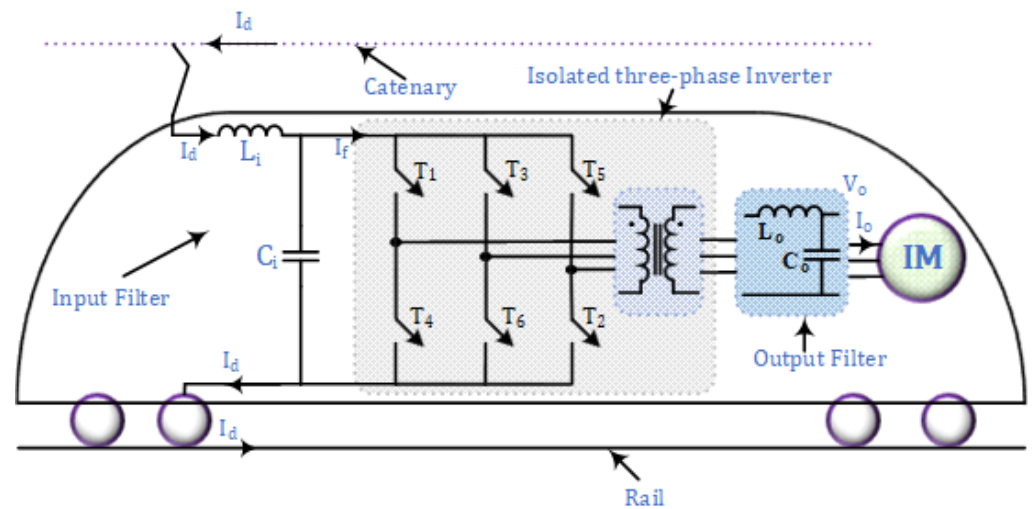


Figure 4. Schematic diagram of an AEPSS circuit structure in a single car.

Table 1. Electrical parameters of the AEPSS.

Parameters	Value
System power	30 kW
Input voltage (range)	550 V _{DC} to 800 V _{DC}
Output voltage	3 phase 380 V _{AC}
Output frequency	60 Hz

The specifications of the components of the AEPSS used in Figure 4 are shown in Table 2. It has a transformer and input and output filters, which are comprised of inductors and capacitors, the input inductor $L_i = 300 \mu\text{H}$, an input capacitor $C_i = 500 \mu\text{F}$, a three-phase transformer ($\Delta - Y$ type) with a turn ratio of 1:1, three output inductors with $L_o = 500 \mu\text{H}$ each, and three output capacitors with $C_o = 200 \mu\text{F}$ each. Since the output voltage is three-phase, it requires three inductors and three capacitors; one set of filters for each phase or a three-phase filter can be deployed to perform the filtering action. In the AEPSS system of medium-capacity (as shown in Figure 4), the ITPI is provided with an isolation transformer in series. The main purpose of this isolation transformer is to isolate the overhead conductor power from the rail vehicle AEPSS output power. Thus, the AEPSS output power is stable and safe for electrical equipment. When the overhead conductor output power or rail vehicle AEPSS output power is unstable, this isolation transformer helps in avoiding any damage to the mainline overhead conductor equipment and the rail vehicle electrical equipment. Therefore, this circuit architecture has been used as the model for testing.

Table 2. The component parameters of the AEPSS.

Parameters	Quantity	Value
Input inductor L_i	1	300 μH
Input capacitor C_i	1	500 μF
Transformer	1	1:1 ($\Delta - Y$), 40 kVA
Output inductor L_o	3	500 μH
Output capacitor C_o	3	200 μF

3. Working Principle of Isolated Three-Phase Inverter

The three-phase inverter (TPI) is an important part of the AEPSS structure, which is used to convert the input DC voltage into AC voltage at the output, which can suitably be used for the desired applications after filtering it. Power semiconductor switches are

used for designing a high-power TPI. These switches may be either metal oxide semiconductor field effect transistors (MOSFET) or insulated gate bipolar transistors (IGBT). The forward voltage drop in the MOSFET is high, which produces a higher conduction loss in it. However, the turn-off time of MOSFET is smaller, which makes it suitable for fast switching. Therefore, the MOSFETs are preferably used for higher switching frequencies (up to a certain MHz). Additionally, they are used in low and medium-power applications due to their lower voltage and current handling capacity. Conversely, the forward voltage drop in the IGBT is low, which causes a lower conduction loss. However, the turn-off time of IGBT is higher, which causes a higher switching loss, making it inappropriate for fast switching. Therefore, the IGBTs are preferably used for lower switching frequencies (up to a few kHz). In addition, they are often used in high-power applications due to their higher voltage and current handling capacity.

Traditional TPIs are designed using six switches. Since this inverter is used for higher-power applications, six IGBTs are used as the switch to design the TPI. These IGBTs require the switching pulse to turn it on and produce the required output. These pulses control the duty cycle (turn-on period of each IGBT) or firing angle and thus adjust the output power. These switching pulses can be generated using any control strategy or any optimization algorithm to produce the best result. A 750 V_{DC} supply is given at the input of TPI through the AEPSS input filter (L_i and C_i). The TPI controller then adopts any control strategy to drive the six IGBTs T_1 , T_2 , T_3 , T_4 , T_5 , and T_6 of the TPI.

The TPI operates in six different operating modes. Figure 5 illustrates the different operating modes of the AEPSS TPI. The conducting IGBTs are shown with a dark black line, while the non-conducting IGBTs are shown with a light black line. The direction of current flow in the circuit is depicted by a dotted pink line. Figure 5a shows the no-operation mode of the TPI, in which none of the IGBTs are conducting, and thus the TPI is in off mode. Figure 5b shows mode-1, in which the IGBTs T_1 , T_5 , and T_6 are conducting, while the IGBTs T_2 , T_3 , and T_4 are not conducting. Consequently, V_a , V_b , and V_c are generated at the output terminal of the TPI. Figure 5c shows mode-2, in which the IGBTs T_1 , T_2 , and T_6 are conducting, while the IGBTs T_3 , T_4 , and T_5 are not conducting. Consequently, V_a , V_b , and V_c are generated at the output terminal of the TPI. Figure 5d shows mode-3, in which the IGBTs T_1 , T_2 , and T_3 are conducting, while the IGBTs T_4 , T_5 , and T_6 are not conducting. Consequently, V_a , V_b , and V_c are generated at the output terminal of the TPI. Figure 5e shows mode-4, in which the IGBTs T_2 , T_3 , and T_4 are conducting, while the IGBTs T_1 , T_5 , and T_6 are not conducting. Consequently, V_a , V_b , and V_c are generated at the output terminal of the TPI. Figure 5f shows mode-5, in which the IGBTs T_3 , T_4 , and T_5 are conducting, while the IGBTs T_1 , T_2 , and T_6 are not conducting. Consequently, V_a , V_b , and V_c are generated at the output terminal of the TPI. Figure 5g shows mode-6 in which the IGBTs T_4 , T_5 , and T_6 are conducting, while the IGBTs T_1 , T_2 , and T_3 are not conducting. Consequently, V_a , V_b , and V_c are generated at the output terminal of the TPI. These six operating modes can also be demonstrated by the switching states for AEPSS TPI in tabular form and are concisely presented in Table 3.

Table 3. Switching states for AEPSS three-phase inverter.

States	T_1	T_2	T_3	T_4	T_5	T_6	V_a	V_b	V_c
Mode-1	1	0	0	0	1	1	+V	−V	+V
Mode-2	1	1	0	0	0	1	+V	−V	−V
Mode-3	1	1	1	0	0	0	+V	+V	−V
Mode-4	0	1	1	1	0	0	−V	+V	−V
Mode-5	0	0	1	1	1	0	−V	+V	+V
Mode-6	0	0	0	1	1	1	−V	−V	+V

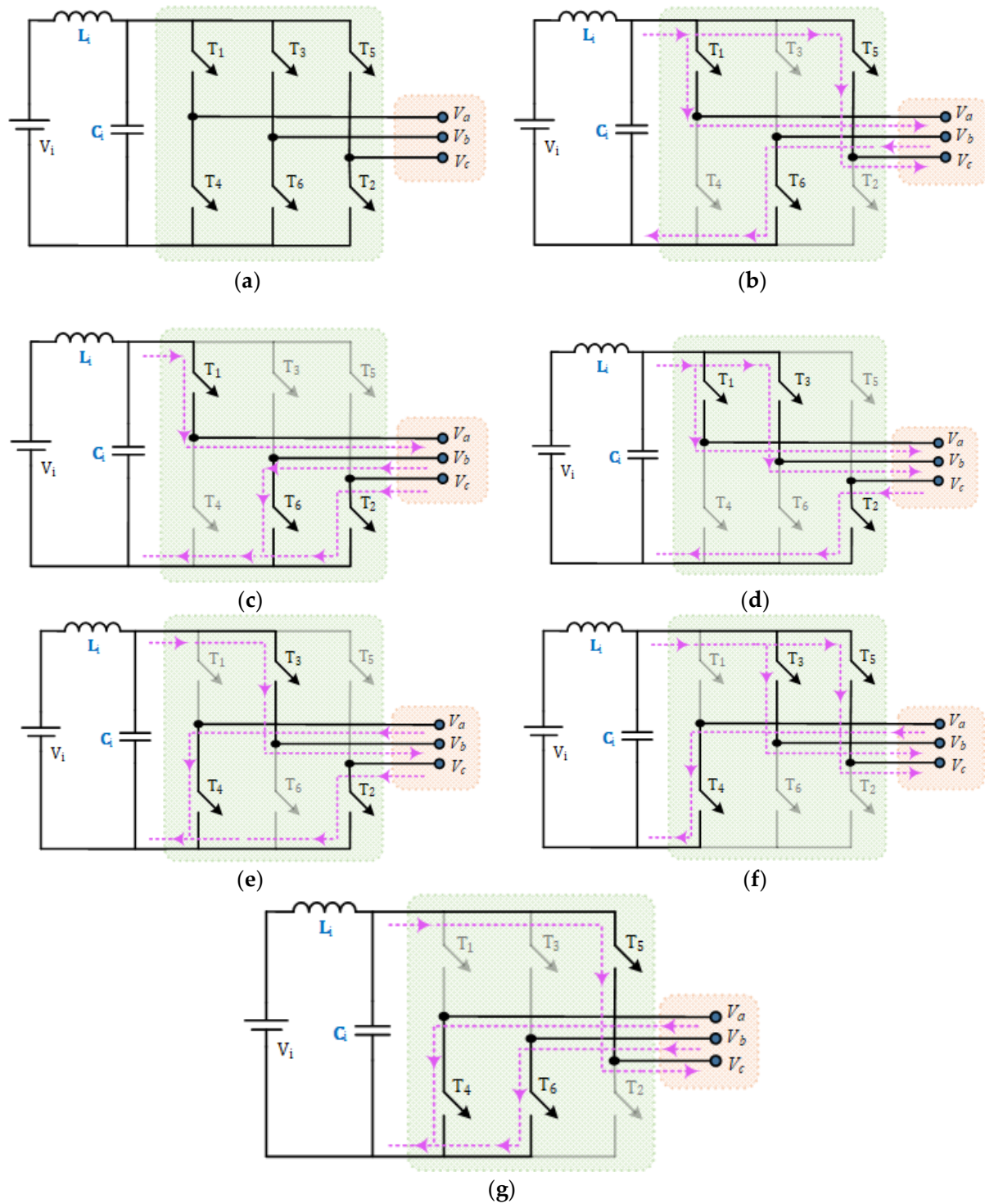


Figure 5. Various operating modes of AEPSS three-phase inverter. (a) No operation; (b) Mode-1; (c) Mode-2; (d) Mode-3; (e) Mode-4; (f) Mode-5; (g) Mode-6.

4. Traditional and Proposed Control Strategy

4.1. Traditional Voltage Cancellation Method

Numerous control strategies and optimization algorithms were proposed in the literature. Depending on the effectiveness, applications, and complexity of the control technique, the most effective and efficient control strategy can be used for switching the IGBTs in the inverters. These switching pulses control the duty cycle of each IGBT and thus produce

the best result. Figure 6 shows the AEPSS architecture diagram with a microcontroller unit (MCU). The control unit employed a microcontroller to produce the switching pulses to control the conduction period of the IGBTs and thus regulate the output voltage. A 750 V_{DC} supply is given at the input of ITPI through the AEPSS input filter (L_i and C_i). The ITPI controller then adopts any control strategy to drive the six IGBTs T_1 , T_2 , T_3 , T_4 , T_5 , and T_6 of the ITPI.

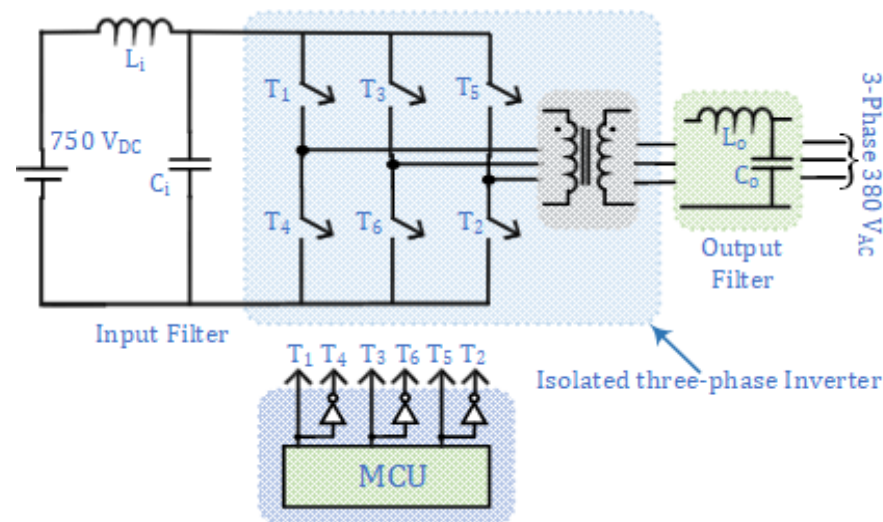


Figure 6. The AEPSS architecture diagram with a control unit.

The traditional voltage cancellation method (VCM) is used in several applications, especially in the AEPSS of rail vehicles. The traditional VCM is often used in rail vehicle systems [11]. It has several advantages. First, this control strategy is simple and easy to maintain. It can shorten the maintenance time and improve the repair rate and availability of the rail vehicle. Second, this method can avoid high-frequency control signals generating high-frequency noise, which affects the performance of other electrical equipment of the rail vehicle. It can cause the electrical equipment of the rail vehicle to perform abnormally, the rail vehicle's other equipment to transient abnormally, or the rail vehicle to stop running. However, it has a few shortcomings. The AEPSS components are bulky and massive, therefore, AEPSS maintenance is time-consuming and laborious.

Figure 7 demonstrates the schematic diagram of AC voltage square waveforms in different lines using the traditional VCM, including the v_a , v_b , v_c , v_{ab} , v_{bc} , and v_{ca} . The MCU in ITPI produces six pulses, each with a turn-on duration of 180 degrees (π radian). The pulse generated for the driver circuit of IGBTs T_1 and T_3 differ by an angle of 120 degrees ($2\pi/3$ radian), and the pulse for the driver circuit of IGBTs T_1 and T_5 differ by an angle of 240 degrees ($4\pi/3$ radian). The pulse generated for the driver circuit of IGBTs T_1 and T_4 are complementary. Similarly, the pulse for IGBTs T_3 and T_6 are complementary. Likewise, the pulse for IGBTs T_2 and T_5 are also complementary.

The ITPI operates in six different modes, and the conduction period of each mode is demonstrated in Figure 7. In mode-1, the conduction period is $0-\beta_1$. In mode-2, the conduction period is $\beta_1-\beta_2$. In mode-3, the conduction period is $\beta_2-\beta_3$. In mode-4, the conduction period is $\beta_3-\beta_4$. In mode-5, the conduction period is $\beta_4-\beta_5$. In mode-6, the conduction period is $\beta_5-\beta_6$. The ITPI generates a three-phase AC voltage which is then isolated and filtered by the transformer and output filter (L_o and C_o), respectively. Finally, the required three-phase 380 V_{AC}/60 Hz output is obtained from the AEPSS, which provides power to electrical appliances in rail vehicles.

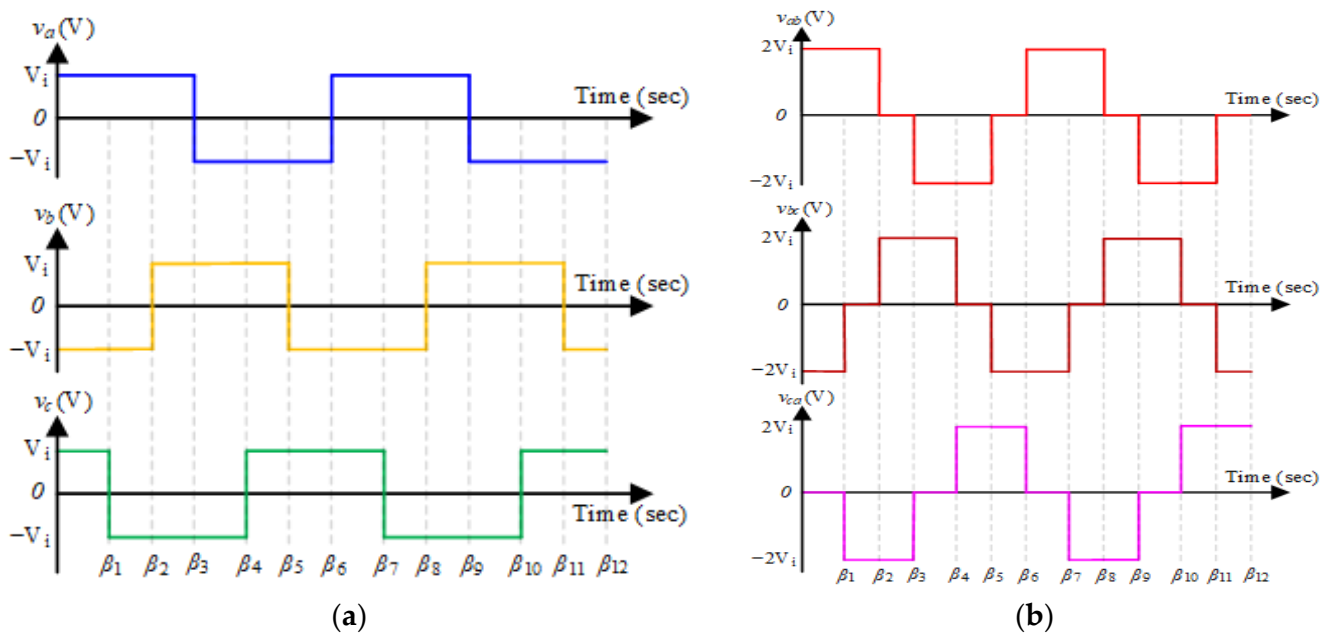


Figure 7. AC voltage square waveforms in different lines by implementing the traditional VCM (a) voltage of each line v_a , v_b , and v_c . (b) Voltage between two lines v_{ab} , v_{bc} , and v_{ca} .

4.2. Proposed Control Strategy

The traditional VCM is often used in the AEPSS of rail vehicles as this control strategy is simple and easy to maintain. However, the output voltage produced using this control strategy suffers from high THD. A few additional components are added to the AEPSS circuit to reduce the THD of the output voltage, which makes the AEPSS components bulky and massive. Additionally, AEPSS maintenance is laborious and time consuming. Therefore, certain strategies have been developed to overcome these shortcomings. The exponential curve-based (ECB) control strategy has been proposed in this study. This control strategy is based on the growth and decay of charge in the RC circuit and the harmonic elimination by detecting the Fourier expansion series of the AEPSS three-phase output voltage level. The proposed control strategy quickly adjusts the duty cycle of each control pulse to reach the best value, which is used to drive the six IGBTs used in the designing of the ITPI. The ITPI produces the output v_a , v_b , and v_c , whose standard range is $380 \text{ V}_{AC} \pm 10\%$. Figure 8 demonstrates the AEPSS architecture diagram using the proposed ECB control strategy. Since v_a , v_b , and v_c are the important parameters to determine the AEPSS output voltage level and the number of voltage harmonics. The proposed control strategy detects these voltages and checks whether the output AC voltage from ITPI is with some abnormality (such as unbalanced three-phase voltage). In the case of some abnormality in any phase, the proposed control strategy does not work. The ITPI generates a three-phase AC power which is isolated and filtered by the transformer and output filter (L_o and C_o). Three-phase $380 \text{ V}_{AC}/60 \text{ Hz}$ from the AEPSS output is then used to provide power for the rail vehicle electrical equipment.

Moreover, the proposed ECB control strategy detects and measures v_{ao} , v_{bo} , and v_{co} . If the AEPSS outputs v_{ao} , v_{bo} , and v_{co} are unbalanced, the proposed control strategy does not work. The proposed control strategy is based on the following three principles:

1. Growth of charge in the series RC circuit;

A series RC circuit is depicted in Figure 9. When the key is at position-1, i.e., the switch is closed, the capacitor starts charging up, and the charging current is maximum due to the entire voltage drop across the resistance R .

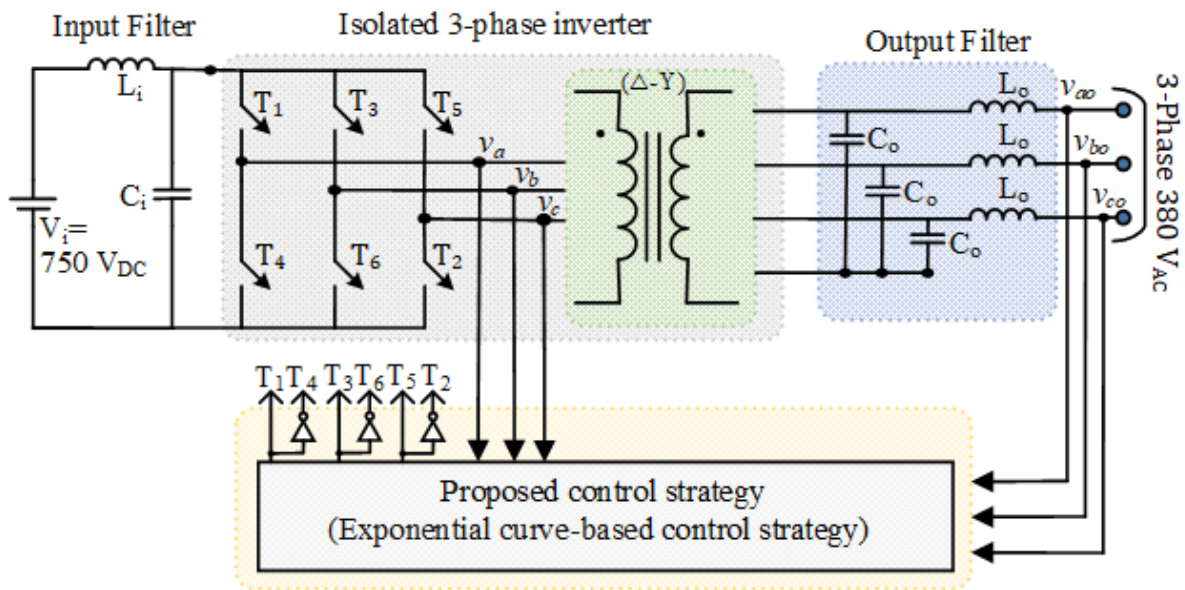


Figure 8. The AEPSS architecture diagram using the proposed exponential curve-based control strategy.

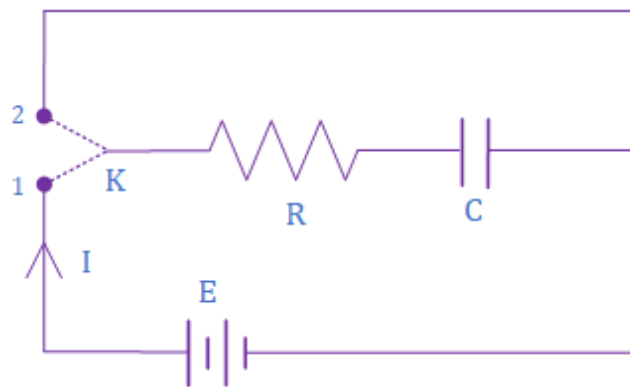


Figure 9. RC Series circuit.

Therefore, the initial charging current,

$$I_0 = E/R \tag{1}$$

At any instant, let the charging current be $I = dQ/dt$

The potential difference across the resistor, $V_R = I \cdot R$

The potential difference across the capacitor, $V_C = Q/C$

According to Kirchoff's voltage law, we have

$$E = Q/C + I \cdot R \tag{2}$$

On simplifying and re-arranging, the above equation can be modified as

$$-\log_e(EC - Q) = \frac{t}{RC} + K \tag{3}$$

where K is the constant of integration,

At $t = 0$, then $Q = 0$

$$K = -\log_e(EC)$$

Therefore, Equation (3) becomes

$$-\log_e(EC - Q) = \frac{t}{RC} - \log_e(EC)$$

On solving this, we obtain

$$Q = Q_0 \left[1 - e^{-\frac{t}{RC}} \right] \quad (4)$$

The quantity $\tau = RC$ is the time constant of the RC circuit. When $t = \tau = RC$ in Equation (4), $Q = 0.632$, $Q_0 = 63.2\%$ of the max. charge. Figure 10 shows the exponential growth of charge in an RC circuit.

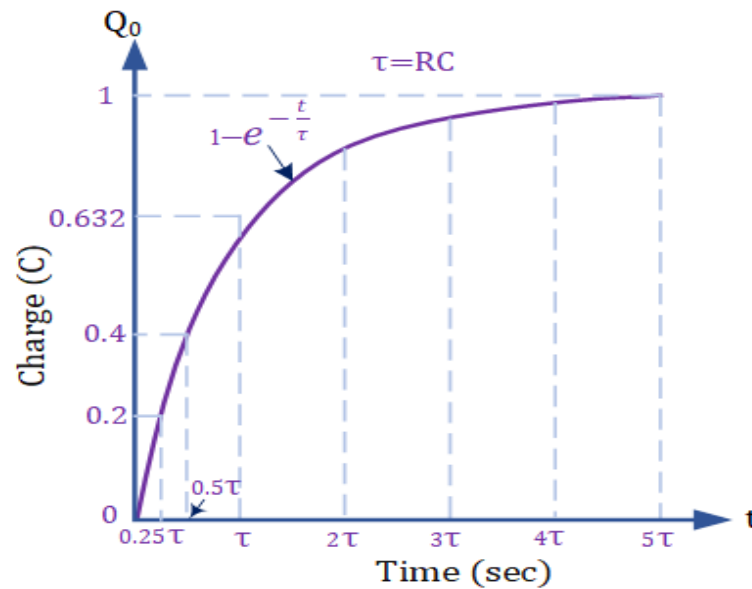


Figure 10. Exponential growth of charge in RC circuit.

2. Decay of charge in the series RC circuit;

Switch position 1 is used to charge the capacitor. After the capacitor is fully charged, the switch is thrown to position-2 to discharge the capacitor through the resistor R . Therefore, initially $Q = Q_0$ (maximum).

After time ' t ', the charges on the capacitor be Q . According to the KVL, we have

$$Q/C + I \cdot R = 0 \quad (5)$$

On simplifying and re-arranging, the above equation can be modified as

$$-\log_e Q = -\frac{t}{RC} + K \quad (6)$$

where K is the constant of integration

At $t = 0$, $Q = Q_0$ and thus, $K = -\log_e(Q_0)$.

Therefore, Equation (6) becomes

$$\log_e Q = -\frac{t}{RC} + \log_e(Q_0)$$

On solving this, we obtain

$$Q = Q_0 \cdot e^{-\frac{t}{RC}} \quad (7)$$

When $t = \tau = RC$ in Equation (7), $Q = Q_0 \cdot e^{-1} = 0.368 Q_0 = 36.8\%$ of the max. charge. Figure 11 shows the decaying of charge in the RC circuit.

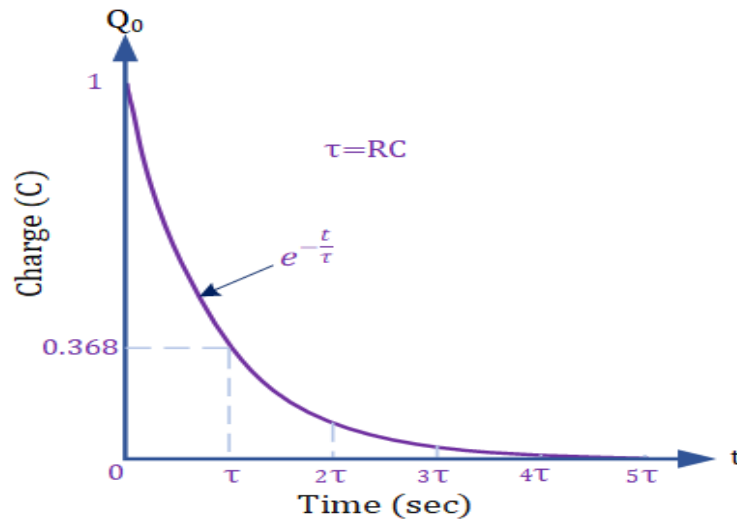


Figure 11. Decaying of charge in a series RC circuit.

3. Harmonic elimination technique;

To reduce the number of harmonics in the exponential output voltage waveform generated by ITPI, the modulation index (MI) is presented in the Fourier expansion series as below. The relationship between the exponential curve voltage waveform and the angle is shown in Figure 12.

$$m = \frac{4}{\pi} [\sin\theta_0 - \sin\theta_1 + \sin\theta_2 - \dots + (-1)^n \sin\theta_n] \tag{8}$$

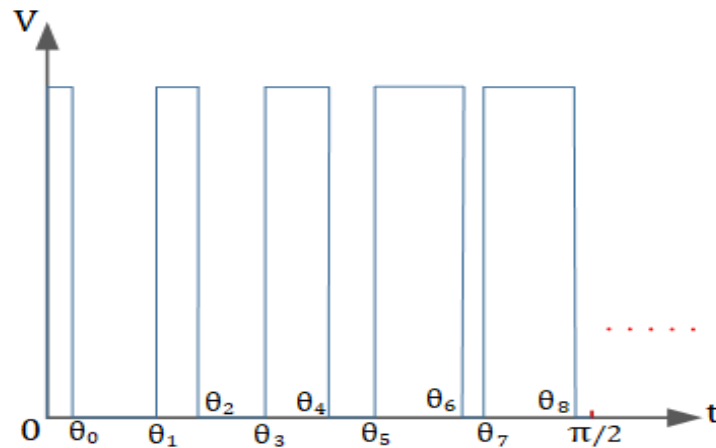


Figure 12. The switching angles for the exponential curve voltage waveform.

Equations (9)–(11) present the equations for eliminating the 3rd, 5th, and nth harmonics from the output voltage. The relationship between Equations (8)–(11) and Figure 12 helps in the adjustment of each duty cycle. Thus, the angle θ between them is used to reduce the harmonic amount.

$$m = \frac{4}{3\pi} [\sin 3\theta_0 - \sin 3\theta_1 + \sin 3\theta_2 - \dots + (-1)^n \sin 3\theta_n] \tag{9}$$

$$m = \frac{4}{5\pi} [\sin 5\theta_0 - \sin 5\theta_1 + \sin 5\theta_2 - \dots + (-1)^n \sin 5\theta_n] \tag{10}$$

$$m = \frac{4}{n\pi} [\sin n\theta_0 - \sin n\theta_1 + \sin n\theta_2 - \dots + (-1)^n \sin n\theta_n] \quad (11)$$

This ECB control strategy is based on the growth and decay of charge in the series RC circuit and the harmonic elimination by detecting the Fourier expansion series of the AEPSS three-phase output voltage level. When the switch is at position 1, the capacitor starts charging due to the growth of charges in it. As soon the switch is thrown to position-2, the capacitor begins to discharge due to the decay of charge in the capacitors. The proposed control strategy is based on this principle which is demonstrated in Figures 9–12. The exponential voltage waveform generation using the proposed control strategy can be categorized into several operating modes and can be described as follows:

Mode-1: The voltage waveform across the capacitor during the charging condition is shown in Figure 10. The voltage waveform is similar to a quarter sine wave from 0 to $\pi/2$. The waveform can be represented by the exponential curve equation. This curve is further divided into five points that help in determining the duty cycle. The curve is parted at 0.25, 0.5, 1, 2, and 4, as shown in Figure 13. The duty cycle D can be determined as;

$$D = 1 - e^{-p} \quad (12)$$

Here, p represents the point of each section of the curve, which are 0.25, 0.5, 1, 2, and 4. Putting the value of p into Equation (12), the duty cycle can be obtained as 0.22, 0.39, 0.632, 0.865, and 0.981. Therefore, the IGBT of ITPI can be operated with the switching pulse of these duty cycles to generate an exponential output waveform from 0 to $\pi/2$.

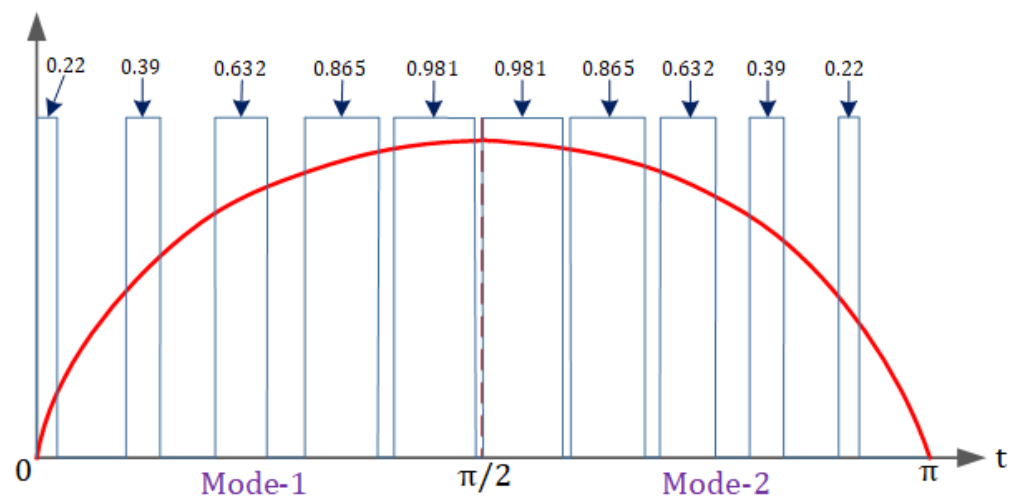


Figure 13. The output duty cycle and corresponding voltage waveform from 0 to π using the proposed exponential curve-based control strategy.

Mode-2: The second quarter of the output waveform is from $\pi/2$ to π . Since the second quarter of the output waveform should be symmetrical to the first quarter, it is necessary to change the parameter p and put its value into Equation (12) to evaluate the duty cycle. During this period, the parameters p are 4, 2, 1, 0.5, and 0.25, respectively. Thus, the corresponding duty cycles are 0.981, 0.865, 0.632, 0.39, and 0.22. Therefore, the IGBT of ITPI can be operated with the switching pulse of these duty cycles to generate an exponential output waveform from $\pi/2$ to π (as shown in Figure 13).

Mode-3: The voltage waveform across the capacitor during the discharging condition is shown in Figure 11. The voltage waveform is similar to a quarter sine wave from π to $3\pi/2$. The waveform can be represented by the exponential curve equation. This curve is

further divided into five points that help in determining the duty cycle. The curve is parted at 0.25, 0.5, 1, 2, and 4, as shown in Figure 14. The duty cycle D can be determined as:

$$D = e^{-p} \quad (13)$$

Here, p represents the point of each section of the curve, which are 0.25, 0.5, 1, 2, and 4. Putting the value of p into Equation (13), the duty cycle can be obtained as 0.77, 0.6, 0.367, 0.135, and 0.018. Therefore, the IGBT of ITPI can be operated with the switching pulse of these duty cycles to generate an exponential output waveform from π to $3\pi/2$.

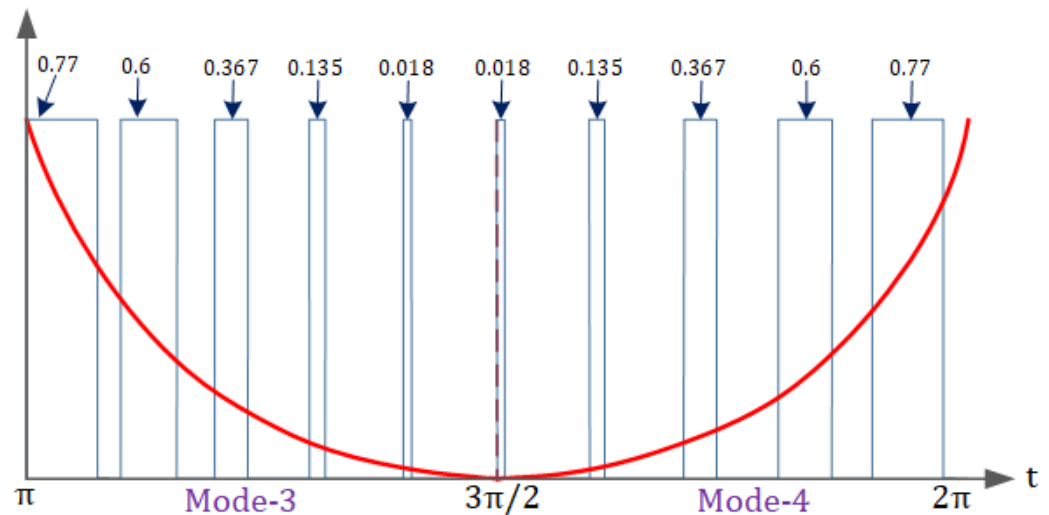


Figure 14. The output duty cycle and corresponding voltage waveform from π to 2π using the proposed exponential curve-based control strategy.

Mode-4: The fourth quarter of the output waveform is from $3\pi/2$ to 2π . Since the fourth quarter of the output waveform should be symmetrical to the third quarter, it is necessary to change the parameter p and put its value into Equation (13) to evaluate the duty cycle. During this period, the parameters p is 4, 2, 1, 0.5, and 0.25, respectively. Thus, the corresponding duty cycles are 0.018, 0.135, 0.367, 0.6, and 0.77. Therefore, the IGBT of ITPI can be operated with the switching pulse of these duty cycles to generate an exponential output waveform from $3\pi/2$ to 2π (as shown in Figure 14). Overall, Equations (12) and (13) are used to control the switching of the IGBTs in the ITPI and thus generating an exponential output voltage waveform.

Later, Equations (12) and (13) are added to the parameter a , and the angle between each duty cycle is adjusted through this parameter a , and Equations (14) and (15) are then used to reduce the harmonic amount. In this study, the parameter a range of 0.1 to 2.

$$D = 1 - e^{-p \cdot a} \quad (14)$$

$$D = e^{-p \cdot a} \quad (15)$$

In this study, the equation for the resonant frequency f_o can be presented in terms of filter capacitor C_o and filter inductor L_o which is expressed as follows.

$$f_o = \frac{1}{2\pi\sqrt{L_o C_o}} \quad (16)$$

4.3. Flowchart

A flowchart is a pictorial representation of the various steps involved in a process. The working of the proposed ECB control strategy can simply be elaborated with a flowchart.

Figure 15 depicts the flow chart of the proposed ECB control strategy for the AEPSS. Initially, the v_a , v_b , v_c , v_{ao} , v_{bo} , and v_{co} are detected and measured. The proposed ECB control strategy produces pulses to drive the IGBTs T_1 to T_6 of the ITPI. The three-phase output from the ITPI is isolated through a transformer and filtered using an output filter. Then, the AEPSS detects v_a , v_b , v_c , v_{ab} , v_{bc} , and v_{ca} , ensuring that the ITPI output is a three-phase 380 V_{AC}/60 Hz. If the output voltage is greater than or smaller than 380 V, MCU manipulates the duty cycle for each switch according to the proposed control strategy. This signal thus helps in controlling the output voltage closer to the desired voltage. This way, the proposed controlling strategy helps in producing a stable and high-quality output voltage.

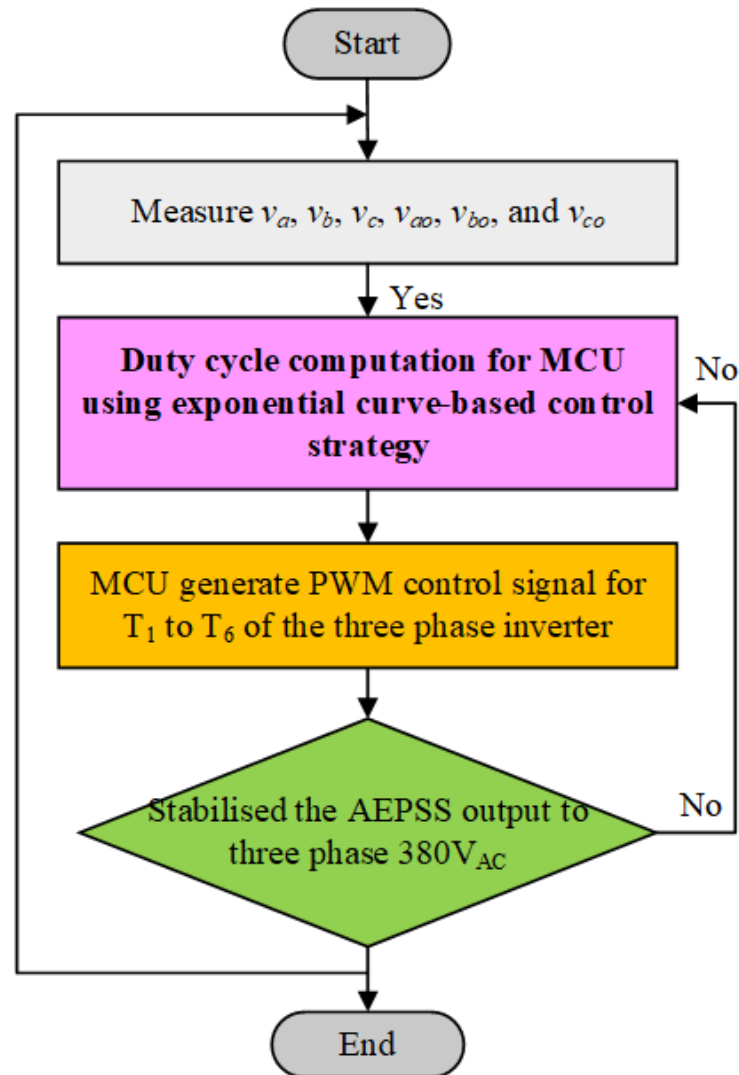


Figure 15. Flowchart of the proposed ECB control strategy in an AEPSS.

5. Experimental Validation

Hardware implementation of the prototype of AEPSS has been performed in the laboratory to validate the proposed exponential curve-based (ECB) control strategy. The laboratory hardware prototype of AEPSS used in this study is displayed in Figure 16. The hardware setup consists of an ITPI designed by employing six IGBT (RGC80TSX8RGC11) with the specification of 1800 V and 80 A. Microcontroller unit dsPIC33FJ64GS606 generates the controlling pulses for the gate of IGBTs. These pulses control the switching time of the IGBT by regulating the pulse width of the signal. These controlling pulses can be generated using different strategies. The traditional VCM and proposed ECB control technique has

been used for this purpose. Afterward, this controlling pulse is transferred to the gate terminal of IGBT through the gate driver circuit employing the TLP250H optocoupler. A 15 V DC supply is required to power the driver circuit, which is provided by a DC power supply.

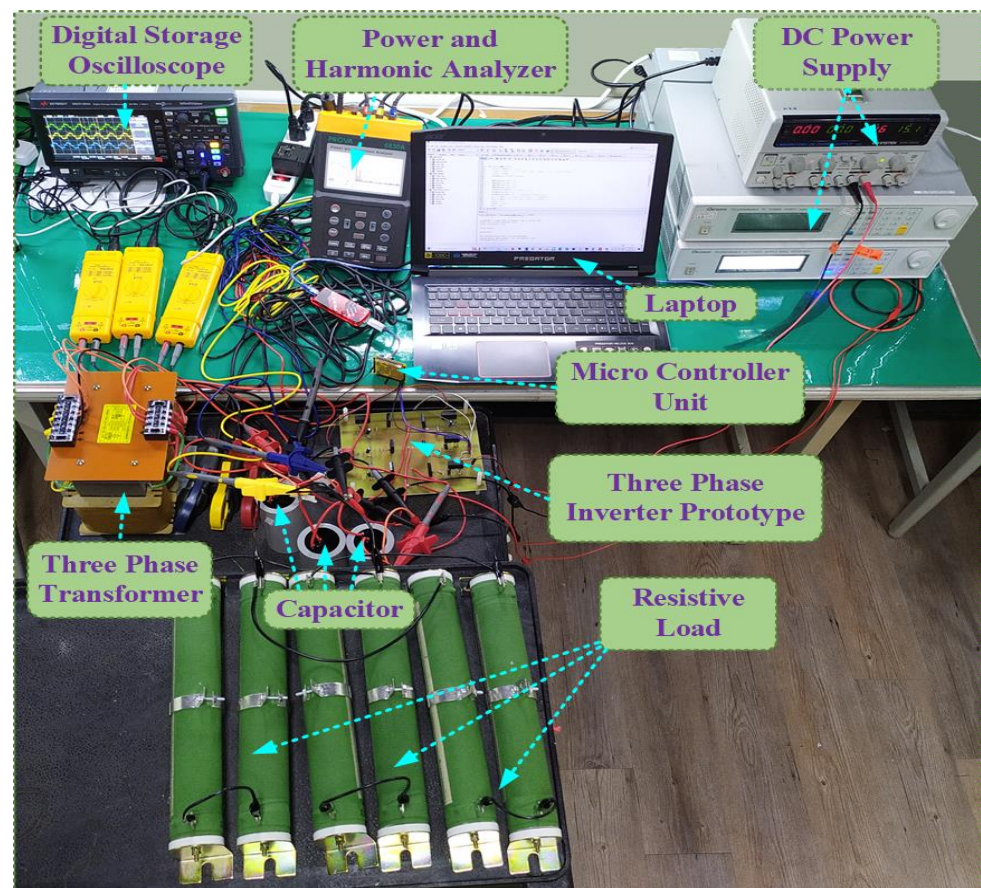


Figure 16. Laboratory hardware prototype of AEPSS in rail vehicles.

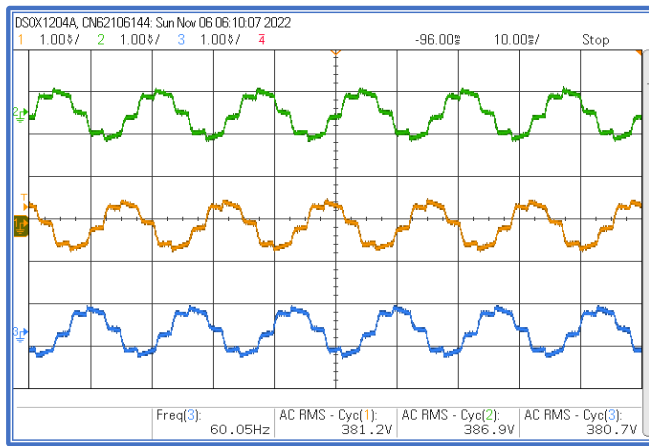
Since a single DC power supply can be used for a voltage up to 600 V only. However, 800 V has been required to perform this experiment. Therefore, two DC supply has been cascaded to increase the voltage specification of the DC supply. After cascading these two dc power supplies, this overall system can provide the DC supply up to 800 V. The three-phase output from the ITPI is then isolated using the transformer (1:1, $\Delta - Y$), and filtered the output voltage by employing a capacitor in each phase to obtain a three-phase 380 V_{AC}/60 Hz output. A load is connected at the output terminal to perform the testing and to evaluate the effectiveness of the traditional VCM and the proposed ECB control strategy. A digital storage oscilloscope has been employed for measuring the output voltage waveform using both the traditional techniques as well as a proposed control technique. A power and harmonic analyzer was used to measure and record the harmonic profile of the output voltage waveform. The specification of the experimental setup is shown in Table 4.

5.1. Hardware Result Using Traditional VCM

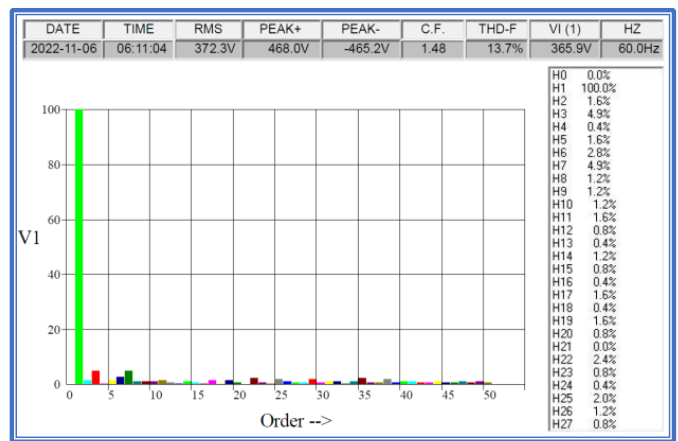
Traditional VCM has been implemented on an AEPSS prototype for rail vehicles at different voltage values. Several conditions are considered here in which voltage ranges from 550 V_{DC} to 800 V_{DC}. The performance of the ITPI was observed with three different voltage conditions, which are 550 V_{DC}, 750 V_{DC}, and 800 V_{DC}, and has been shown in Figures 17–19.

Table 4. Specifications of the laboratory hardware setup.

Equipment/Components	Quantity	Specification
Microcontroller unit	1	Microchip, dsPIC33FJ64GS606
Three-phase transformer	1	1:1 ($\Delta - Y$), 3 kVA
Three-phase inverter	1	$V_i = 550 V_{DC} \sim 800 V_{DC}$, $V_o = 380 V_{AC}$, 3 kVA
Resistive load	3	$500 + 100 + 50 \Omega$, 3 kVA
Capacitor	3	200 μF , 500 μF , 450 V_{AC}
IGBT	6	ROHM, RGC80TSX8RGC11
Gate Driver Circuits	6	TOSHIBA, TLP 250H
Power and harmonic analyzer	1	PROVA, 6830A
Digital storage oscilloscope	1	KEYSIGHT, DSOX1204A
Laptop	1	Acer, Predator Helios 300
DC power supply	2	CHROMA, 62012P
DC power supply	1	GWINSTEK, GPS-4303

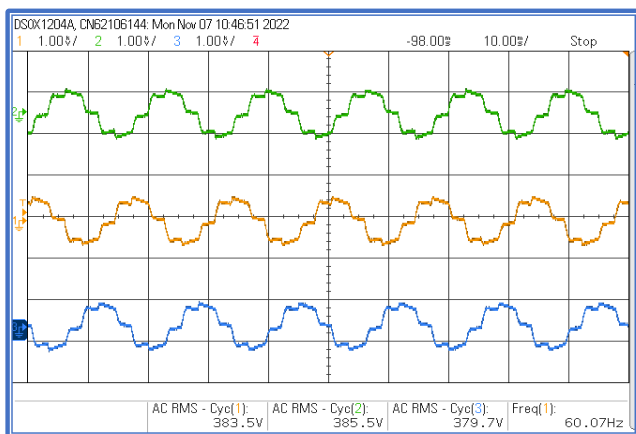


(a)

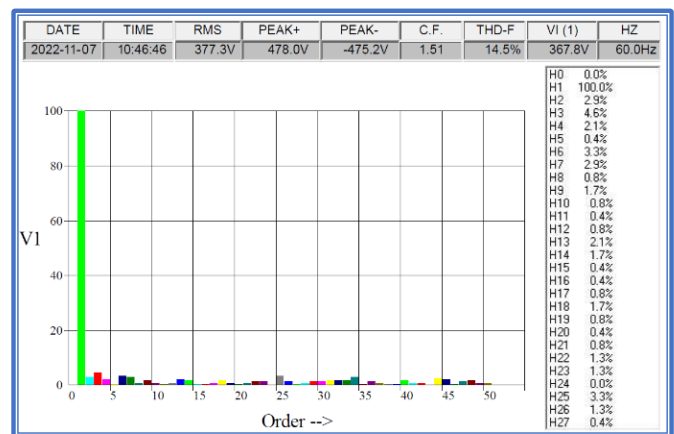


(b)

Figure 17. Experimental result of the traditional VCM for the AEPSS with $V_i = 550 V_{DC}$ (a) V_o waveform (b) Harmonic profile of V_o .



(a)



(b)

Figure 18. Experimental result of the traditional VCM for the AEPSS with $V_i = 750 V_{DC}$ (a) V_o waveform (b) Harmonic profile of V_o .

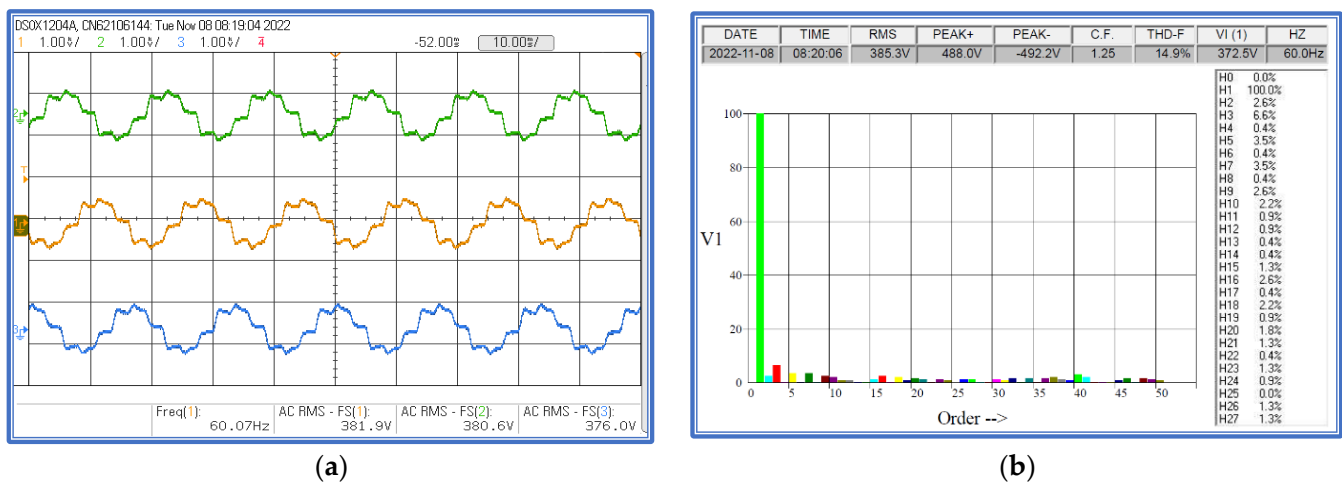


Figure 19. Experimental result of the traditional VCM for the AEPSS with $V_i = 800 V_{DC}$ (a) V_o waveform (b) Harmonic profile of V_o .

Figure 17 shows the experimental result of the traditional VCM for the AEPSS, with an input voltage of $550 V_{DC}$. The output is supplied to a three-phase resistive load with $R = 650 \Omega$ in each phase. The output voltage V_o and harmonic profile of output voltage are demonstrated in Figure 17. The three-phase output of the ITPI is shown in Figure 17a. The orange waveform depicts the output voltage in phase I whose RMS value is $381.2 V_{AC}$. The green waveform shows the output voltage in phase II, whose RMS value is $386.9 V_{AC}$ and the blue waveform shows the output voltage in phase III whose RMS value is $380.7 V_{AC}$. The frequency of the output voltage is 60 Hz. The harmonic profile of output voltage V_o is illustrated in Figure 17b. It shows that the RMS value of voltage in phase I is $372.3 V_{AC}$, the positive peak voltage is 468.0 V, the negative peak voltage is $-465.2 V$, and the THD of output voltage in phase I is 13.7%. The fundamental frequency of output voltage is 60 Hz.

The output voltage V_o and harmonic profile of output voltage by the implementation of the traditional VCM with the input voltage $V_i = 750 V_{DC}$ are shown in Figure 18. The three-phase output of the ITPI is shown in Figure 18a. The orange waveform shows the output voltage in phase I whose RMS value is $383.5 V_{AC}$. The green waveform depicts the output voltage in phase II, whose RMS value is $385.5 V_{AC}$ and the blue waveform shows the output voltage in phase III whose RMS value is $379.7 V_{AC}$. The frequency of the output voltage is 60 Hz. The harmonic profile of output voltage V_o is illustrated in Figure 18b. It shows that the RMS value of voltage in phase I is $377.8 V_{AC}$, the positive peak voltage is 478.0 V, the negative peak voltage is $-475.2 V$, and the THD of output voltage in phase I is 14.5%. The fundamental frequency of output voltage is 60 Hz.

The output voltage V_o and harmonic profile of output voltage by the implementation of the traditional VCM with the input voltage $V_i = 800 V_{DC}$ are shown in Figure 19. The three-phase output of the ITPI is shown in Figure 19a. The orange waveform shows the output voltage in phase I whose RMS value is $381.9 V_{AC}$. The green waveform depicts the output voltage in phase II, whose RMS value is $380.6 V_{AC}$ and the blue waveform shows the output voltage in phase III whose RMS value is $376.0 V_{AC}$. The frequency of the output voltage is 60 Hz. The harmonic profile of output voltage V_o is illustrated in Figure 19b. It shows that the RMS value of voltage in phase I is $385.3 V_{AC}$, the positive peak voltage is 488.0 V, the negative peak voltage is $-492.2 V$, and the THD of output voltage in phase I is 14.9%. The fundamental frequency of output voltage is 60 Hz.

5.2. Hardware Result Using Proposed Control Strategy

From the previous section, it is obvious that the THD of the output voltage is high using the traditional VCM on the AEPSS prototype for rail vehicles at different voltage values. This can be seen in Figures 17–19. This high value of THD may cause several issues

in the AEPSS of the rail vehicle. Therefore, the proposed exponential curve-based (ECB) control strategy has been implemented on an AEPSS prototype at different voltage values. The performance of the ITPI was observed with three different voltage conditions, 550 V_{DC}, 750 V_{DC}, and 800 V_{DC}, as shown in Figures 20–22.

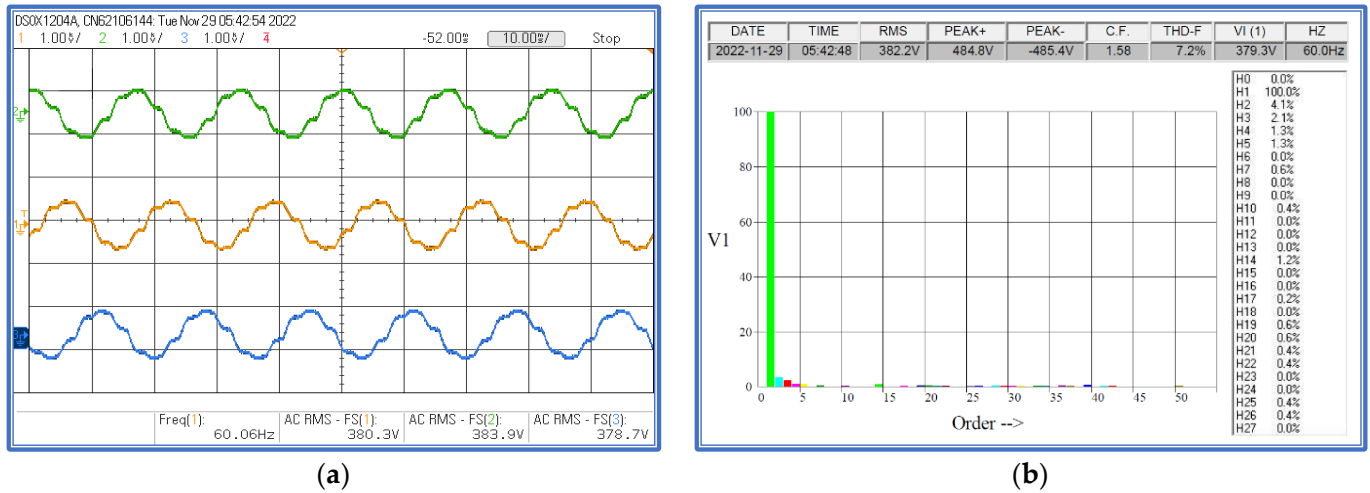


Figure 20. Experimental result of the proposed ECB control strategy for the AEPSS with $V_i = 550 V_{DC}$ (a) V_o waveform (b) Harmonic profile of V_o .

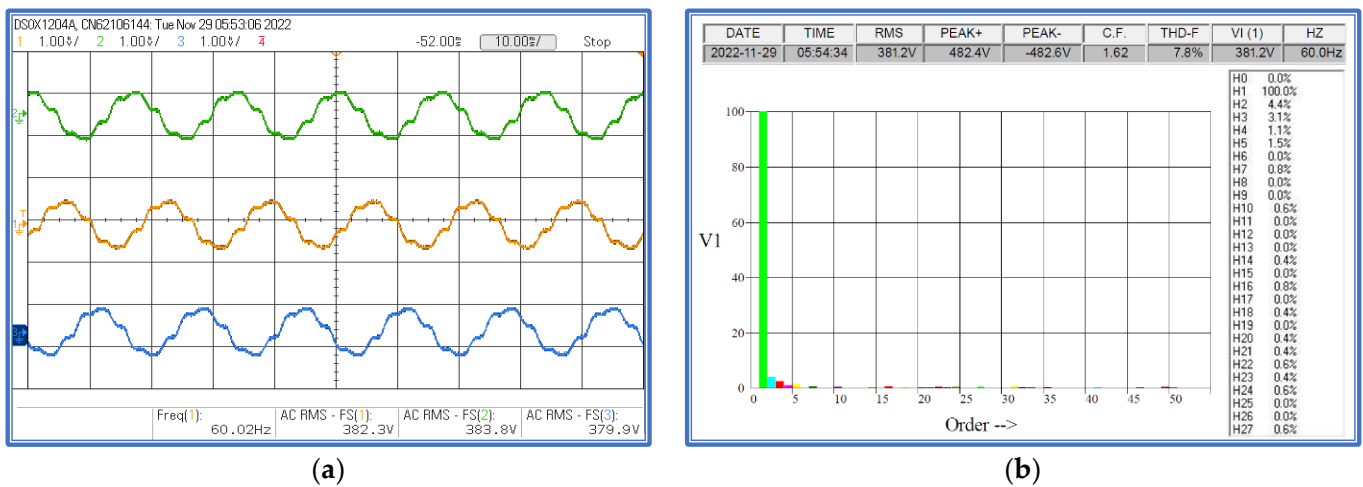


Figure 21. Experimental result of the proposed ECB control strategy for the AEPSS with $V_i = 750 V_{DC}$ (a) V_o waveform (b) Harmonic profile of V_o .

The result obtained by the implementation of the proposed ECB control strategy with the input voltage $V_i = 550 V_{DC}$ has been demonstrated in Figure 20. The output is supplied to a three-phase resistive load with $R = 650 \Omega$ in each phase. The output voltage V_o and harmonic profile of output voltage have been shown in Figure 20. The three-phase output of the ITPI is illustrated in Figure 20a. The orange waveform shows the output voltage in phase I whose RMS value is 380.3 V_{AC}. The green waveform depicts the output voltage in phase II, whose RMS value is 383.9 V_{AC} and the blue waveform shows the output voltage in phase III whose RMS value is 378.7 V_{AC}. The frequency of the output voltage is 60 Hz. The harmonic profile of output voltage V_o is depicted in Figure 20b. It shows that the RMS value of voltage in phase I is 382.2 V_{AC}, the positive peak voltage is 484.8 V, the negative peak voltage is -485.5 V, and the THD of output voltage in phase I is 7.2%. The fundamental frequency of output voltage is 60 Hz.

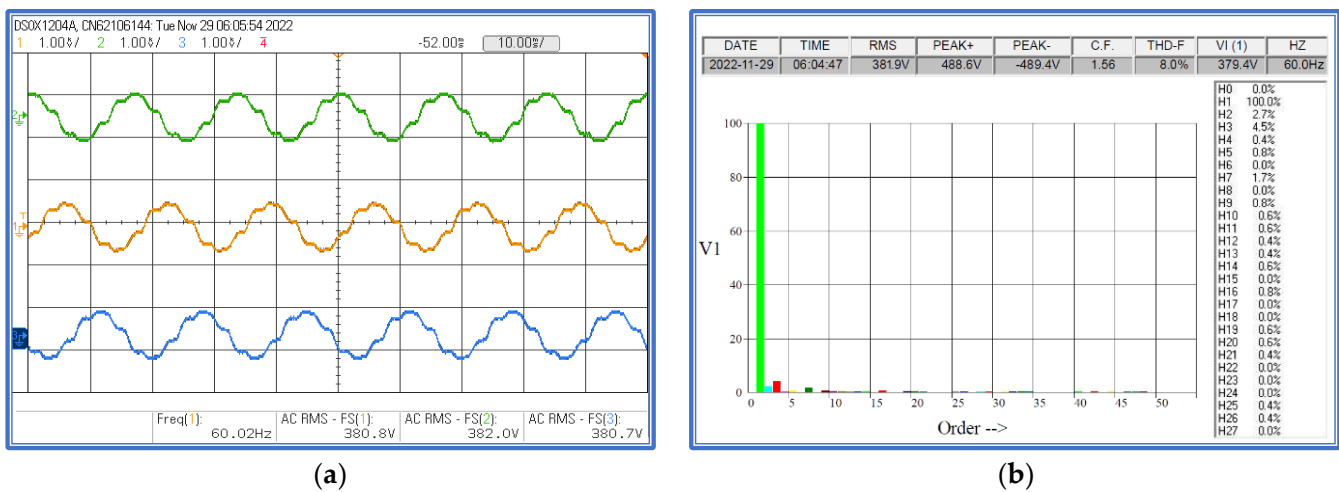


Figure 22. Experimental result of the proposed ECB control strategy for the AEPSS with $V_i = 800 V_{DC}$ (a) V_o waveform (b) Harmonic profile of V_o .

The output voltage V_o and harmonic profile of output voltage by the implementation of the proposed ECB control strategy with the input voltage $V_i = 750 V_{DC}$ are shown in Figure 21. The three-phase output of the ITPI is illustrated in Figure 21a. The orange waveform shows the output voltage in phase I whose RMS value is $382.3 V_{AC}$. The green waveform depicts the output voltage in phase II, whose RMS value is $383.8 V_{AC}$, and the blue waveform shows the output voltage in phase III whose RMS value is $379.9 V_{AC}$. The frequency of the output voltage is 60 Hz. The harmonic profile of output voltage V_o is depicted in Figure 21b. It shows that the RMS value of voltage in phase I is $381.2 V_{AC}$, the positive peak voltage is 482.4 V, the negative peak voltage is 482.6 V, and the THD of output voltage in phase I is 7.8%. The fundamental frequency of output voltage is 60 Hz.

The output voltage V_o and harmonic profile of output voltage by the implementation of the proposed ECB control strategy with the input voltage $V_i = 800 V_{DC}$ are shown in Figure 22. The three-phase output of the ITPI is illustrated in Figure 22a. The orange waveform shows the output voltage in phase I whose RMS value is $380.8 V_{AC}$. The green waveform depicts the output voltage in phase II, whose RMS value is $382.0 V_{AC}$, and the blue waveform shows the output voltage in phase III whose RMS value is $380.7 V_{AC}$. The frequency of the output voltage is 60 Hz. The harmonic profile of output voltage V_o is depicted in Figure 22b. It shows that the RMS value of voltage in phase I is $381.9 V_{AC}$, the positive peak voltage is 488.6 V, the negative peak voltage is $-489.4 V$, and the THD of output voltage in phase I is 8.0%. The fundamental frequency of output voltage is 60 Hz.

5.3. Comparison of AEPSS Performance Using Both Control Strategies

The performance of the rail vehicle AEPSS can be altered in different ways. Hardware modification in the system can improve the system's performance. However, system modification will be time consuming. It will also add to the weight and cost of the system. Using different control strategies is another way to bolster the system's effectiveness. Therefore, the ECB control strategy has been proposed in this work. A comparison of the experimental results of the proposed ECB control strategy and traditional VCM is depicted in Figure 23. These control techniques are tested under three different conditions. A comparison of the AEPSS output voltage harmonics using the traditional VCM and the proposed ECB control strategy is shown in Figure 23a. (i) When input voltage $V_i = 550 V_{DC}$, the THD is 13.7% and 7.2% for the traditional VCM and proposed ECB control strategy, respectively. (ii) When input voltage $V_i = 750 V_{DC}$, the THD is 14.5% and 7.8% for the traditional VCM and proposed ECB control strategy, respectively. (iii) When input voltage $V_i = 800 V_{DC}$, the THD is 14.9% and 8.0% for the traditional VCM and proposed ECB control strategy, respectively. Additionally, the THD of the AEPSS increases with an increase in the

input voltage. However, it can be concluded that the THD is enormously reduced using the proposed ECB control strategy.

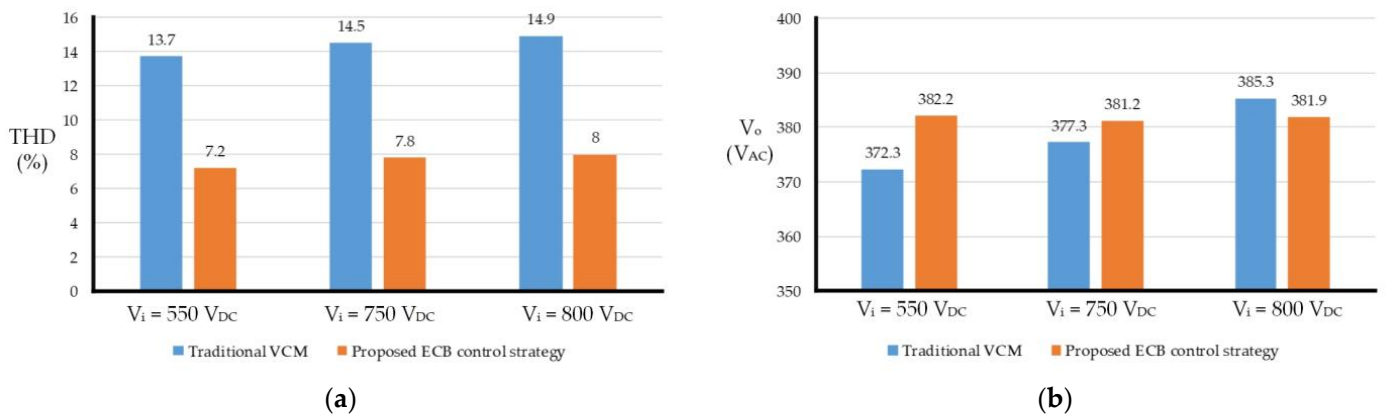


Figure 23. Comparison of the experimental result of the proposed ECB control strategy and traditional VCM: (a) voltage THD and (b) output voltage level.

Figure 23b demonstrates the comparison of the AEPSS output voltage V_o using the two control strategies. (i) When input voltage $V_i = 550 \text{ V}_{DC}$, the output voltage V_o is 372.3 V_{AC} and 382.2 V_{AC} , respectively, for the traditional and proposed control strategy. (ii) When input voltage $V_i = 750 \text{ V}_{DC}$, the output voltage V_o is 377.3 V_{AC} and 381.2 V_{AC} , respectively, for the traditional and proposed control strategy. (iii) When input voltage $V_i = 800 \text{ V}_{DC}$, the output voltage V_o is 385.3 V_{AC} and 381.9 V_{AC} , respectively, for the traditional and proposed control strategies. It is evident from the table that the output voltage V_o is more stable and closer to the required output voltage, even with the change in the input voltage using the proposed control strategy. However, the variation in the output voltage V_o is more on using the traditional control strategy.

During the implementation of the proposed ECB control strategy and the traditional control strategy in the laboratory on the hardware prototype, the output filter volume of the AEPSS is different, which is obvious from Table 5. In the proposed ECB control strategy, the filter has capacitor $C_o = 200 \mu\text{F}$ while the filter has capacitor $C_o = 500 \mu\text{F}$ in the traditional control strategy. Hence, the size of the AEPSS output filter using the proposed ECB control strategy is smaller than the traditional control strategy. This will not only reduce the system volume but also reduce the system cost.

Table 5. Comparison of the AEPSS filter size using the two control strategies.

Control Strategy	Capacitor Value (μF)
Traditional VCM	500
Proposed ECB control strategy	200

From the result, it is obvious that the output voltage harmonics and output voltage level for the proposed ECB control strategy are superior to the traditional control strategy. In addition, the filter size is also reduced.

6. Conclusions

A comparison of the AEPSS output performance using the traditional VCM and the proposed ECB control strategy was performed. These control strategies are tested under three different conditions, i.e., $V_i = 550 \text{ V}_{DC}$, 750 V_{DC} , and 800 V_{DC} . The THD is 13.7%, 14.5%, and 14.9% using the traditional control strategy and 7.2%, 7.8%, and 8.0% using the proposed ECB control strategy, respectively, with input voltage 550 V_{DC} , 750 V_{DC} , and 800 V_{DC} during hardware implementation. This result shows that the THD is enormously reduced using the proposed ECB control strategy. The output voltage V_o is

372.3 V_{AC}, 377.3 V_{AC}, and 385.3 V_{AC} by implementing the traditional control strategy and 382.2 V_{AC}, 381.2 V_{AC}, and 381.9 V_{AC} using the proposed ECB control strategy, respectively, for 550 V_{DC}, 750 V_{DC}, and 800 V_{DC} input voltage during the hardware implementation. This shows that the output voltage V_o is more stable and closer to the required output using the proposed ECB control strategy even though the input voltage is changed. During the hardware implementation, the capacitor was deployed as the output filter with C_o = 500 μF for the traditional control strategy and C_o = 200 μF using the proposed ECB control strategy. The size of the AEPSS output filter using the proposed ECB control strategy is smaller than the traditional control strategy. This will not only reduce the system volume but also reduce the system cost.

Author Contributions: Conceptualization, S.A.F., H.-D.L. and C.-H.L.; Formal analysis, S.A.F. and H.-D.L.; Investigation, S.A.F. and H.-D.L.; Methodology, S.A.F., H.-D.L. and C.-H.L.; Supervision, S.-D.L.; Writing—original draft, S.A.F., C.-H.L., S.-D.L., H.-D.L., A.S. and L.-Y.H.; Writing—review & editing, S.A.F., C.-H.L., S.-D.L., H.-D.L., A.S. and L.-Y.H. all authors provided critical feedback and helped in the research, analysis, and manuscript. All authors have read and agreed to the published version of the manuscript.

Funding: The authors gratefully acknowledge the financial support of the Ministry of Science and Technology of Taiwan, under contract number of MOST 111-2221-E-167-004. This work was also supported by the National Taiwan Normal University Subsidy Policy for International Collaboration and Research Projects.

Data Availability Statement: Not applicable.

Conflicts of Interest: The authors declare no conflict of interest.

References

1. Lin, B.-R. Bidirectional Resonant Converter for DC Microgrid Applications. *Processes* **2021**, *9*, 1664. [CrossRef]
2. Atawi, I.E.; Hendawi, E.; Zaid, S.A. Analysis and Design of a Standalone Electric Vehicle Charging Station Supplied by Photovoltaic Energy. *Processes* **2021**, *9*, 1246. [CrossRef]
3. Liu, H.-D.; Farooqui, S.-A.; Lu, S.-D.; Lee, Y.-L.; Lin, C.-H. A Novel SLOPDM Solar Maximum Power Point Tracking Control Strategy for the Solar Photovoltaic Power System. *Processes* **2022**, *10*, 1452. [CrossRef]
4. Khan, A.I.; Khan, R.A.; Farooqui, S.A.; Sarfraz, M. Artificial Neural Network-Based Maximum Power Point Tracking Method with the Improved Effectiveness of Standalone Photovoltaic System. In *AI and Machine Learning Paradigms for Health Monitoring System*; Springer: Singapore, 2021; pp. 459–470.
5. Castillo, O.; Álvarez, R.; Domingo, R. Opportunities and Barriers of Hydrogen–Electric Hybrid Powertrain Vans: A Systematic Literature Review. *Processes* **2020**, *8*, 1261. [CrossRef]
6. Wangai, A.W.; Rohacs, D.; Boros, A. Supporting the Sustainable Development of Railway Transport in Developing Countries. *Sustainability* **2020**, *12*, 3572. [CrossRef]
7. Electric Vehicles Are Not Just the Wave of the Future, They Are Saving Lives Today. *Earthjustice*. 2020. Available online: <https://earthjustice.org/features/electric-vehicles-explainer> (accessed on 12 December 2022).
8. Various Advantages of Electric Cars—Conserve Energy Future. *Conserve Energy Future*. Available online: <https://www.conserve-energy-future.com/advantages-and-disadvantages-of-electric-cars.php> (accessed on 12 December 2022).
9. Central Organization for Railway Electrification. Available online: https://core.indianrailways.gov.in/view_section.jsp?lang=0&id=0,294,302,538 (accessed on 12 December 2022).
10. Krastev, I.; Tricoli, P.; Hillmansen, S.; Chen, M. Future of Electric Railways: Advanced Electrification Systems with Static Converters for ac Railways. *IEEE Electr. Mag.* **2016**, *4*, 6–14. [CrossRef]
11. Verdicchio, A.; Ladoux, P.; Caron, H.; Courtois, C. New Medium-Voltage DC Railway Electrification System. *IEEE Trans. Transp. Electr.* **2018**, *4*, 591–604. [CrossRef]
12. Spiriyagin, M.; Cole, C.; Sun, Y.Q.; McClanachan, M.; Spiriyagin, V.; McSweeney, T. *Design and Simulation of Rail Vehicles*; CRC Press: Boca Raton, FL, USA, 2014.
13. Hitachi Rail Inc. *Training Materials Propulsion and Auxiliary Power System*; Hitachi Rail Inc.: Pistoia, Italy, 2020.
14. Siemens Inc. *Training Materials Auxiliary Power System*; Siemens Inc.: Berlin, Germany, 2008.
15. Salam, M.A.; Rahman, Q.M. *Fundamentals of Electrical Circuit Analysis*; Springer: Singapore, 2018.

16. Farooqui, S.A.; Shees, M.M.; Alsharekh, M.F.; Alyahya, S.; Khan, R.A.; Sarwar, A.; Islam, M.; Khan, S. Crystal structure algorithm (CryStAl) based selective harmonic elimination modulation in a cascaded h-bridge multilevel inverter. *Electronics* **2021**, *10*, 3070. [[CrossRef](#)]
17. Khan, R.A.; Farooqui, S.A.; Sarwar, M.I.; Ahmad, S.; Tariq, M.; Sarwar, A.; Zaid, M.; Ahmad, S.; Mohamed, A.S.N. Archimedes optimization algorithm based selective harmonic elimination in a cascaded h-bridge multilevel inverter. *Sustainability* **2021**, *14*, 310. [[CrossRef](#)]
18. De la Fuente, E.P.; Mazumder, S.K.; Franco, I.G. Railway Electrical Smart Grids: An introduction to next-generation railway power systems and their operation. *IEEE Electr. Mag.* **2014**, *2*, 49–55. [[CrossRef](#)]

Disclaimer/Publisher's Note: The statements, opinions and data contained in all publications are solely those of the individual author(s) and contributor(s) and not of MDPI and/or the editor(s). MDPI and/or the editor(s) disclaim responsibility for any injury to people or property resulting from any ideas, methods, instructions or products referred to in the content.